HEFAT2010
7th International Conference on Heat Transfer, Fluid Mechanics and Thermodynamics
19-21 July 2010
Antalya, Turkey

MODELING OF BUBBLE FLOW DISTRIBUTION IN CRYSTAL SUSPENDED NON-NEWTONIAN FLUIDS

N. M. S. Hassan[1*], M. M. K. Khan[2] and M. G. Rasul[2]
[1]Process Engineering & Light Metals (PELM) Centre
Faculty of Sciences, Engineering and Health
CQUniversity, Rockhampton, Queensland, 4702, AUSTRALIA
[2]College of Engineering and Built Environment
Faculty of Sciences, Engineering and Health
CQUniversity, Rockhampton, Queensland, 4702, AUSTRALIA
[*1]Corresponding author, Email: n.hassan@cqu.edu.au

ABSTRACT

This paper investigates a computational study of air bubbles rising in massecuite equivalent non-Newtonian crystal suspensions. Bubble rise motion inside the stagnant liquid of 0.05% xanthan gum crystal suspension was investigated and modelled using computational fluid dynamics (CFD) model to gain an insight into the bubble flow distribution. CFD code FLUENT was used for numerical simulation and bubble rise characteristics were computed through a Volume of Fluid (VOF) model. The influences of the Reynolds number (Re) along with other dimensionless groups such the Weber number (*We*), and the Eötvös number (*Eo*) on bubble velocity and bubble trajectory are discussed. The effects of the vortices on bubble velocity distribution are analyzed. The simulated results of the bubble flow contours were validated by the experimental results. The model developed is capable of predicting the entire flow characteristics of different sizes of bubble inside the liquid column.

INTRODUCTION

Bubbles rising in non-Newtonian polymer liquids have been studied for many years due to their importance in many engineering applications such as fermentation, floatation, and waste water treatment. The rise characteristics of a bubble are dominated by the physical properties of the fluids, as well as the surrounding flow field. And for most cases, they are difficult to envisage using simple criteria or analytical formula.

The bubbles are used in vacuum pan operation in sugar industries which is an important process for the production of raw sugar. The high grade massecuites - a fluid made from sugar crystals and mother sugar syrup (molasses) is important for processing raw sugar [1]. In sugar factories, vacuum pans are used to process the massecuite. Within the vacuum pans, bubbles play an important role by producing very strong circulation within the vessel. A solution of sugar and water is passed into a vacuum pan during the sugar refinement process and the solution is heated to evaporate water and concentrate the sugar solution to aid crystallization [2].

Air bubble disperses into the liquid phase is very complex two phase flow problems. One of the basic examples of two-phase flows is studying dynamics of a single air bubble rising in a liquid column [3, 4]. The most important characteristic of two-phase flow is the existence of interfaces, which separate the phases and the associated discontinuities in the properties across the phase interfaces. Because of the deformable nature of gas-liquid and liquid-liquid interfaces, a considerable number of interface configurations are possible. Consequently, the various heat and mass transfers that occur between a two-phase mixture and a surrounding surface, as well as between the two phases, depend strongly on the two phase flow regimes. In order to have a better understanding of the interaction between the two-phase flows, the air-liquid system is being performed with a CFD code-FLUENT 6.3.

Among available simulation approaches in 'FLUENT' software, the Volume of Fluid (VOF) method is one of the most eminent surface-tracking techniques in which the motion of all phases is modelled by solving a single set of momentum equations and tracking the volume fraction of each fluid throughout the domain [5, 6]. Hirt and Nichols [7] originally developed the VOF technique which is used in this study.

In this present work, a numerical study with the VOF model has been investigated to study the bubble flow characteristics in water and crystal suspension for different bubble sizes. The influences of the dimensionless quantities such as the Reynolds number, (Re), the Weber number, (*We*) and the Eötvös number (*Eo*) on bubble rise velocity and trajectory are discussed. Simulation results are also compared with the experimental data.

NOMENCLATURE

Re	[-]	Reynolds number
We	[-]	Weber number
Eo	[-]	Eötvös number
g	[m/s^2]	Acceleration due to gravity
$\vec{u}$	[-]	Velocity vector
p	[N/m^2]	Pressure
τ	[N/m^2]	Viscous stress tensor
F_{sf}	[N/m^3]	Surface tension force
t	[s]	Time
Co	[-]	Dimensionless number
Δx	[m]	Grid size
Δt	[-]	Time step
∇	[-]	Gradient (Nabla) operator
α_1	[-]	Volume fraction of liquid
α_2	[-]	Volume fraction of Gas

Greek letters

$\Delta\rho$	[kg/m^3]	Density difference between liquid and air bubble
ρ_1	[kg/m^3]	Liquid density
ρ_2	[kg/m^3]	Gas density
σ	[N/m]	Surface tension
μ	[Pa.s]	Apparent viscosity
μ_1	[Pa s]	Viscosity of liquid phase
μ_2	[Pa s]	Viscosity of gas phase

NUMERICAL APPROACHES

In the two phase flow, the finite-volume VOF approach can model two immiscible fluids (gas-liquid) by solving a single set of momentum equations and tracking the volume fraction of each of the fluids throughout the domain [8]. The VOF model resolves the transient motion of the gas and liquid phase and accounts for the topology changes of the gas (air)-liquid interface induced by the relative motion between the dispersed air bubble and the surrounding liquid [5]. The motion of air-liquid interface is tracked based on the distribution of α_2, the volume fraction of gas in a computational cell, where $\alpha_2 = 0$ in the liquid phase and $\alpha_2 = 1$ in the gas phase. Therefore, the gas-liquid interface exists in the cell where α_2 lies between 0 and 1.

The VOF approach is used to simulate bubble motion based on the Navier – Stokes equations, which are given for the mixture phase. The continuity equation is as follows,

$$\frac{\partial(\rho)}{\partial} + \nabla \cdot (\rho\vec{u}) = 0 \qquad (1)$$

In this study, the flow is governed by a single momentum equation which is solved throughout the entire domain, and the resulting velocity is shared among the phases. The momentum equation is dependent on the volume fractions of all phases through the properties and is given by,

$$\frac{\partial}{\partial t}(\rho\vec{u}) + \nabla\cdot(\rho\vec{u}\vec{u}) = -\nabla p + \nabla\cdot\tau + \rho g + F_{sf}$$
$$\tau = \mu\left(\nabla\vec{u} + \nabla\vec{u}^{T}\right) \qquad (2)$$

Where $\vec{u}$ is velocity vector, p is the pressure, τ is the viscous stress tensor, g is the gravitational force, ρ is the density and μ is the viscosity. The source term F_{sf}, is the surface tension force which is acting on the air – liquid interface.

Surface tension arises along through an interface due to a result of attractive forces between molecules in a fluid. In regions where two fluids (air bubble – liquid) are separated, the surface tension acts to minimize free energy by decreasing the area of the interface. The addition of surface tension to the VOF calculation results in a source term in the momentum equation. The surface tension model in FLUENT is calculated as the continuum surface force (CSF) model originally proposed by Brackbill *et al.* [9].

It is noted that the source term is added on only one side of the interface where the volume fraction calculation is being performed. In Fluent's VOF model, this corresponds to the secondary phase.

The motion of the interface between two immiscible fluids (air bubble and liquid) of different density and viscosity is tracked by the solution of a continuity equation for the volume fraction of the gas, is as follows,

$$\frac{\partial(\alpha_2)}{\partial t} + \vec{u}\cdot\nabla\alpha_2 = 0 \qquad (3)$$

The volume fraction equation is not solved for the primary phase (liquid). The primary phase volume fraction is computed based on the following limit,

$$\alpha_2 + \alpha_1 = 1 \qquad (4)$$

The properties of air and liquid in the transport equations are determined by the presence of the component phases in each volume. In a gas-liquid system, the volume fraction of the secondary phase (gas) is being tracked and the mixture properties of the gas and liquid phases based on the volume fraction weighted average are used. The density and viscosity in each cell at interface are calculated by the following equations:

$$\rho = \alpha_2\rho_2 + (1-\alpha_2)\rho_1 \qquad (5)$$

$$\mu = \alpha_2\mu_2 + (1-\alpha_2)\mu_1 \qquad (6)$$

SOLVER APPROACH

A 2D pressure based-segregated solver with first order unsteady formulation was used for the two-phase modelling in this study. Geo-Reconstruct, a time dependent with the geometric reconstruction interpolation scheme in FLUENT was applied for the time–accurate transient behaviour of the VOF

solution and the 2nd order up-wind differencing scheme was used to overcome numerical diffusion. The pressure-implicit with splitting operators (PISO) pressure-velocity-coupling scheme was used for usual transient calculations. PISO scheme allows for a rapid rate convergence without a significant loss of solution stability and accuracy [6]. Pressure was discretized with a PRESTO scheme because of its strong convergence capability. An implicit body force treatment was also included with this model to improve solution convergence by accounting for the partial equilibrium of the pressure gradient and body force in the momentum equation. In the present computations, an explicit time marching scheme was chosen for solving the volume fraction for the gas and a variable time step (Δt) based on a maximum Courant number (Co) of 0.25 was used for momentum and pressure equations. Co is a dimensionless number that compares the time step in a calculation to the characteristic time of transit of a fluid element across a control volume [8]. A value of 1×10^{-5} was chosen for the time throughout the entire simulations.

Simulations were performed for 2D bubble column with different column diameter for different bubble sizes. Therefore the different geometry was created for different bubbles. A typical mesh was presented for a 2mL volume bubble in Figure. 1.

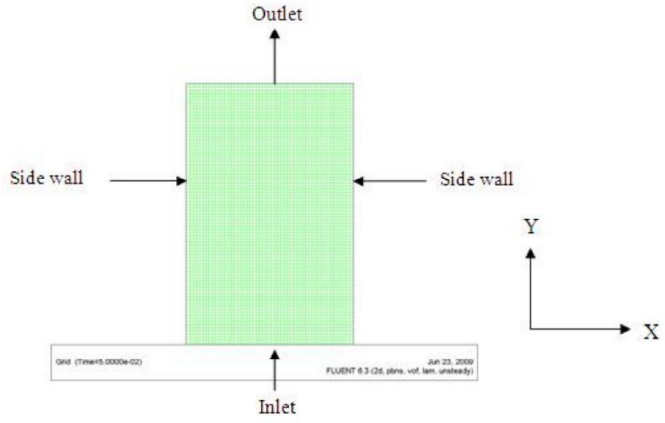

Figure 1 The mesh of two dimensional bubble column.

Simulations were run for different mesh sizes for establishing grid independence. At the side walls, no slip boundary condition was applied. At inlet and outlet, the VELOCITY_INLET and PRESUURE_OUTLET boundary conditions were imposed respectively. The bubble column was designed as an open system, so the operating pressure in the gas space above the liquid column was equal to the atmospheric pressure (101,325 Pa) and the gravitational force, g was equal to -9.81 m/s^2 along with Y axis.

MATERIALS

Two liquids - water and crystal suspensions were used in this study. The crystal suspension was made of 0.05% concentration of xanthan gum (by weight) with 1% (by weight) of 0.23 mm polystyrene crystal particles. The rheological properties for the solutions were measured using an Advanced Rheometric Expansion System (ARES) with a bob and cup geometry [10, 11, 12, 13].

RESULTS AND DISCUSSION

Bubble velocity

The bubble rise characteristics were determined numerically for three bubble sizes (5.76 mm, 15.63 mm and 21.21 mm) in water and crystal suspension. To reduce wall influence, the geometry was constructed considering that the ratio of the bubble diameter to column diameter was smaller than 0.125. Within this limit, the bubble rise velocity is to be independent of wall effects [14].

Hassan et al. [12, 13, 15] carried out detailed experimental investigations of the bubble velocities rising in water and crystal suspensions. Therefore, the validation of simulation results would be based on these experimental data.

The calculated average bubble velocities of numerical and experimental for three bubble sizes were summarized in Table 1.

Table 1 Comparison between experimental and simulation average bubble velocity

Fluid	Bubble size, (mm)	Average bubble velocity (m/s): Experimental	Average bubble velocity(m/s): Simulation	Average differences (%)
Water	5.76	0.2352	0.2379	1.15
Water	15.63	0.2800	0.2978	5.98
Water	21.21	0.3100	0.336	7.73
Crystal	5.76	0.2263	0.2270	0.31
Crystal	15.63	0.2567	0.2470	3.79
Crystal	21.21	0.2960	0.2790	6.08

It is seen from Table 1 that the bubble velocity increases with the increase in bubble diameter which is in accordance with the experimental observations [10, 15]. The differences between experimental and numerical data for smaller bubble (D_b= 5.76) were observed small for both water and crystal suspensions however the difference increases with the increase in bubble diameter. As shown in Table 1, the maximum difference between the experimental and the numerical bubble velocity was observed 7.73% for 21.21 mm bubble in water. This is due to the large fluctuations of the bubble rise velocity because larger bubbles change their shape in time and they also deform more as they rise upward. Greater differences were also observed for larger bubble in comparison with the smaller one in xanthan gum crystal suspension. The average differences in water for all bubble sizes showed higher in comparison with crystal suspension. This is due to the bubble flow in water for larger bubbles are turbulent in nature (1350.73 < Re <6555.58). Hence the bubble velocity oscillates more causing changes shape and trajectory when they rise in water.

In this study, the overall numerical simulation results for all liquids showed some deviations with the experimental ones because of using the high density and viscosity differences in air–liquid system. However, the predicted simulation results are in very good agreement with the experiment and lie within 10% limits.

Bubble trajectory

The comparison results of 5.76mm bubble between experimental and simulated trajectories are shown in Figure 2 for different liquids when predicted over a height of 0.5m from the point of air injection. Figure 2 shows the deviation of bubble from its release point as it rises through water and crystal suspension.

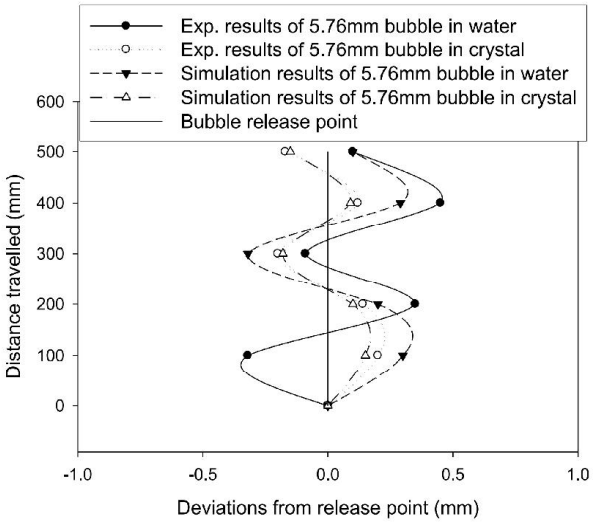

Figure 2 Comparison between experimental and simulation results of rise trajectories for 5.76 mm bubble.

As seen from Figure 2, the smaller bubble of 5.76 mm size deviated horizontally more in water than in crystal suspension and the bubble showed a zigzag motion. The horizontal movement and the zigzag motion in crystal suspension were observed less than that in water. The least movement is due to increased viscosity of the crystal suspension resulting in higher friction on their surface. This phenomenon agrees well with the experimental findings of Hassan et al. [11, 12, 13, 15].

The zigzag motion is due to an interaction between the instability of the straight trajectory and periodic oscillation of the wake. The periodic oscillation of the wake is somewhat less in the crystal suspension due to increase in viscosity. When simulated results are compared with the experimental ones, a similar phenomenon is observed for water and crystal suspension as seen in Figure 2.

The experimental and simulated trajectory results of 15.63 mm bubble are shown in Fig. 3 for all liquids. The bubble of 15.63 mm initially followed a spiral motion and finally, attained a zigzag path for water. On the other hand, for crystal suspension, bubble initially followed straight path, attained its terminal velocity and shape, and then it changed to zigzag motion and finally, switched to spiral motion. As seen from figure 3, the simulated results show a similar trend in comparison with the experimental results.

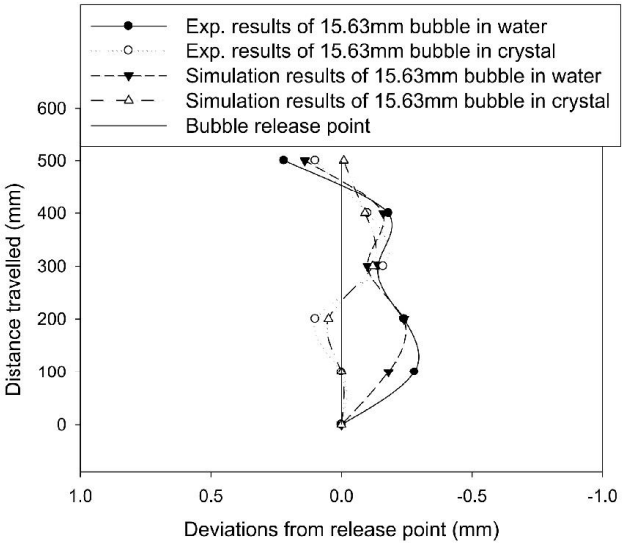

Figure 3 Comparison between experimental and simulation results of rise trajectories for 15.63 mm bubble.

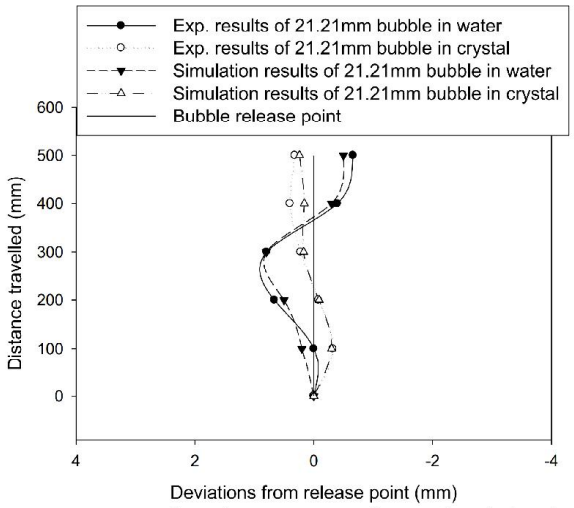

Figure 4 Comparison between experimental and simulation results of rise trajectories for 21.21 mm bubble.

The trajectory experimental and simulated results for 21.21 mm bubbles are plotted in Figure 4. Experimental observations indicate that the 21.21 mm bubbles initially choose the zigzag motion, and finally switch to a spiral path for all liquids. The transition from zigzag to spiral motion is also observed by Aybers and Tapucu [16] as the bubble size increases. As seen from Figure 4, the simulated results show a similar fashion in comparison with the experimental results

Influences of Re, We, Eo and Aspect ratio on bubble velocity and trajectory

Viscosity has a great effect on smaller bubble when the $Re \leq 0.1$ [14]. In this study, viscous forces were shown to have little effect on the bubble rise velocity over the conditions investigated for both in water and crystal suspension which are illustrated in Table 2. For water and crystal suspension, bubble

velocity increases with the increase in Re . At low *We* and *Eo* , surface tension forces were shown to have a greater effect than viscous effects on smaller bubbles (bubble size: 5.76mm). An observation of the intermediate ranges of *We* and *Eo* showed both surface tension and inertia forces had a strong influence on the bubble rise velocity. However, for the larger bubbles investigated at high *We* and *Eo* (bubble size:21.21mm), inertia forces dominated the bubble rise velocity, and surface tension and viscous forces were shown to be less important. Again, at higher Eo, the bubbles showed noticeable deformation, and turned into ellipsoidal and subsequently spherical cap shape.

Table 2 calculated dimensionless quantity in water and crystal suspension

Fluid	Bubble size, mm	Re	We	Eo
Water	5.76	1350.73	4.35	4.44
Water	15.63	4363.41	16.7	32.68
water	21.21	6555.58	27.8	60.18
Crystal	5.76	45.78	4.33	4.77
Crystal	15.63	102.06	15.1	35.16
Crystal	21.21	150.37	27.3	64.74

The Re and *We* have a great influence on bubble trajectory. At low Re and *We* for smaller bubbles (5.76 mm), the bubble showed a zigzag trajectory. For the intermediate region, the bubble of size 15.63 mm showed both zigzag and spiral trajectories in water and crystal suspension. At moderately high *We* and Re , the bubbles deformed and changed from spherical to ellipsoidal and experienced more surface tension and inertia force which induced both zigzag and spiral trajectories. The effect of wake shedding influences the bubble to induce a spiralling rising motion.

Effects of vortices on bubble flow distribution

The typical results of the bubble image, velocity vectors and vorticity magnitudes for three sizes of bubbles in crystal suspension are shown in Figure 5, Figure 6 and Figure 7 respectively. The results of velocity vectors and vorticity magnitudes in water were not shown in this study as these were described elsewhere [17, 18].

In this study, the liquid phase and the gas phase were completely at rest initially in computer simulations. A liquid jet forms at the bottom of the bubble when a single bubble rises due to the buoyancy force in a liquid medium. This jet has a tendency to push the bubble at its lower surface towards the top surface [19, 20]. The pressure gradient at the lower surface of the bubble is greater than the one at the top surface of the bubble. Due to this pressure differences, the vortex sheet develops at the surface. This vortex sheet has a sense of rotation which induces the motion of a liquid jet that pushes into the bubble from below [20]. Hence the deformations of the bubble take place. Eventually, the smaller bubbles face less deformation than their larger counterpart. The arrow shows the velocity at each point and the colour shows the vorticity around the bubble image.

This vortex shedding is caused when a fluid flows past a bubble. The fluid flow past the bubble creates alternating low-pressure vortices on the downstream side of the bubble. Hence, the bubble tends to move toward the low-pressure zone. In this case, the density difference between bubble and the liquid was quite large and the smaller bubble (5.76mm) was deviated horizontally and moved in a zigzag way. It is seen from Fig. 5 that the maximum vorticity was located at the back of the bubble and no re-circular region was formed.

As seen from Figure 6 and Figure 7, the bubble experienced a lateral force and torque along its path when larger bubbles rose in crystal suspension and two strong counter-rotating trailing vortices appeared behind the bubble, hence its path transition occurred which is consistent with findings of Mougin and Magnaudet [21].

It is seen from Figure 7 that the main and secondary vortices were observed for larger bubble of 21.21mm. Thus, in case of viscous flows of crystal suspension, the vorticity was diffused throughout the flow field in comparison with water.

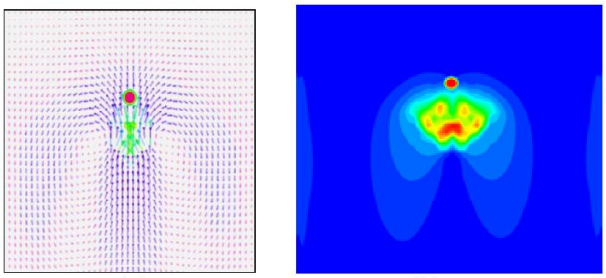

(a) (b)

Figure 5 (a) Velocity vector (b) vorticity magnitude of 5.76 mm bubble in crystal suspension.

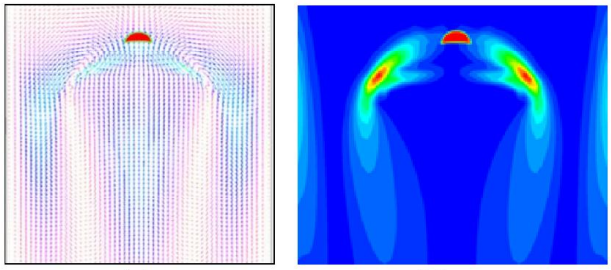

(a) (b)

Figure 6 (a) Velocity vector (b) vorticity magnitude of 15.63 mm bubble in crystal suspension.

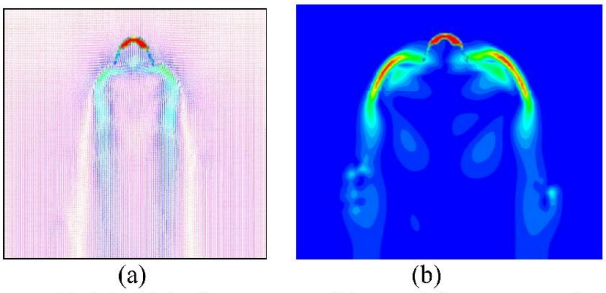

(a) (b)

Figure 7 (a) Velocity vector (b) vorticity magnitude of 21.21mm bubble in crystal suspension.

CONCLUSIONS

In this study, computer simulations have been carried out using the VOF method to study the bubble velocity distributions and trajectory calculations in water and crystal suspension. The simulated bubble velocities were compared with experimental data. A good agreement was observed with the experimental data. Smaller bubble (D_b – 5.76 mm) in water, and crystal suspension showed less numerical differences in comparison with the larger bubble (D_b =21.21mm). This is due to the large fluctuations observed in bubble velocity than seen in smaller ones.

The smaller bubbles (5.76 mm) exhibited the most horizontal movement in water and the least in crystal suspension. The least movement is due to increased viscosity of the crystal suspension resulting in higher friction on their surface. The larger bubbles (15.63mm and 21.21mm) produced more spiral motion in crystal suspension than that of water. Because they experience more resistance on top and deform as their size increases, resulting in spiral motion. Wake shedding also influences the larger bubbles to induce a spiralling motion.

The bubble flow distributions around the bubble are also investigated. In smaller bubble, the maximum vorticity was located at the back of the bubble and no re-circular region was formed.

For larger bubbles (15.63mm and 21.21mm), two strong counter-rotating trailing vortices appeared behind the bubble, hence these bubbles produced path transition. Again, the main and secondary vortices were observed for bubble size of 21.21mm. Thus, in case of viscous flows of crystal suspension, the vorticity was diffused throughout the flow field in comparison with water.

REFERENCES

[1] Broadfoot, R., Miller K. F. and McLaughlin, R. L., Rheology of High Grade Massecuites, Proc. Aust. Soc. Sugar Cane Technocol., 1998, 20, pp. 388 -397.

[2] Rackemann, D. W., Evaluation of Circulation and Heat Transfer in Calandria Tubes of Crystallisation Vacuum Pans, M.Sc. Eng.Thesis,James Cook University, 2005.

[3] Liao, C. B. and Chen, C. H., 2006, Three-Dimensional Numerical Simulation of a Rising Bubble using Level Set Method, Vol. 14(4), No. 53, pp. 483-495.

[4] Hua, J., Stene, J. F. and Lin, P., 2007, Numerical simulation of Gas Bubbles Rising in Viscous liquids at High Reynolds Number, 6th international Conference on Multiphase Flow, ICMF 2007, Leipzig, Germany.

[5] Krisshna, R. and van Baten, J. M., Rise Characteristics of Gas Bubbles in a 2D Rectangular Column: VOF Simulations vs. Experiments, Int. Comm. Heat Mass Transfer, 1999, Vol. 26, No. 7, pp. 965-974.

[6] Delnoij, E., Kuipers, J. A. M and. van Swaaij, W. P. M., Computational fluid dynamics applied to gas-liquid contactors, Chemical Engineering Science, 1997, Vol. 52, No. 21-22, pp.3623-3638.

[7] Hirt, C. W and Nichols B. D., Volume of Fluid (VOF) Method for the Dynamics of Free Boundaries, Journal of Computational Physics,1981, Vol. 39, pp. 201-255.

[8] FLUENT User's guide, 2006.

[9] Brackbill, J. U., Kothe, D. B and Zemarch, C., A Continuu Method for Modelling Surface Tension, J. Comput. Phys., 1992, Vol. 100, pp. 335 – 354.

[10] Hassan, N. M. S., Khan, M. M. K., Rasul, M. G. and Rackemann, D. W., An Experimental Study of Bubble Rise Characteristics in non–Newtonian (Power-Law) Fluids, Proceedings of the 16thAustralasian Fluid Mechanics Conference, Gold Coast, Australia, 2007, pp.1315-1320.

[11] Hassan, N. M. S., Khan, M. M. K., Rasul, M. G., Characteristics of air Bubble Rising in Low Concentration Polymer Solutions, WSEAS TRANSACTIONS on FLUID Mechanics, 2007, Vol. 2, Issue. 3.

[12] Hassan, N. M. S., Khan, M. M. K., Rasul, M. G., An Investigation of Bubble Trajectory and Drag Co-efficient in Water and Non-Newtonian Fluids, WSEAS TRANSACTIONS on FLUID Mechanics, 2008, Vol. 3, Issue. 3.

[13] Hassan, N. M. S., Khan, M. M. K., Rasul, M. G. and Rackemann, D. W., An Experimental Investigation of Bubble Rise Characteristics in a Crystal Suspended non – Newtonian Fluid, Proceedings of the XVth International Congress on Rheology, 80th Annual Meeting, American Institute of Physics (AIP), Monterey, California, USA. ISBN 978-07354-0550-9, 2008, pp. 743-745.

[14] Clift, R., Grace, J. R. and Weber, M. E., 1978, Bubbles, Drops and Particles, Academic Press, 1978, republished by Dover, 2005.

[15] Hassan, N. M. S., Khan, M. M. K., Rasul, M. G., Air Bubble Trajectories in Polymeric Solutions and Crystal Suspensions, Proceedings of the 4th BSME-ASME International Conference on Thermal Engineering, Dhaka, Bangladesh, ISBN 984-300-002844-0, 2008, pp. 970- 975.

[16] Aybers, N. M. and. Tapacu, A., The motion of gas rising through a stagnant liquid, Warme-und Stoffubertragung, 1969, 2, pp. 118-128.

[17]Hassan, N. M. S., Khan, M. M. K., Rasul, M. G. and Subaschandar, N., A Sustainable Production in Sugar Industries: Study of an Improved Vacuum Pan Performance through Numerical Simulations, Proceedings of the Central Region Engineering Conference on Regional Sustainability: Local Solutions to Global Issues, 14th -15th August, 2009, Rockhampton, Australia.

[18] Hassan, N. M. S., Khan, M. M. K, Rasul, M. G. and Subaschandar, N., Modelling of Air Bubble Rising in Water and Polymeric Solution, Proceedings of the 10th Asian International Conference on Fluid Machinery, 21st – 23rd October, 2009, Malaysia.

[19] W. L. Shew, S. Poncet, and J. F., Pinton, Viscoelastic Effects on the Dynamics of a Rising Bubble, Journal. of Statistical Mechanics, 2006, P01009.

[20] Chen, L., Garimella, V. S., Reizes, J.A. and Leonardi, E., Journal of Fluid Mechanics, 1999, vol. 387, pp 61-96, Cambridge University Press.

[21] Mougin, G. and Magnaudet, J., Wake-induced forces and torques on a zigzagging/spiralling bubble, J. Fluid Mech., 2006, 567, pp. 185-194.